Bulge Formation by the Coalescence of Giant Clumps in Primordial Disk Galaxies

Bruce G. Elmegreen

IBM Research Division, T.J. Watson Research Center, 1101 Kitchawan Road, Yorktown Heights, NY 10598, USA

bge@us.ibm.com

Frédéric Bournaud

Laboratoire AIM, CEA-Saclay DSM/IRFU/SAP - CNRS - Université Paris Diderot, F-91191 Gif-sur-Yvette Cedex, France

frederic.bournaud@cea.fr

Debra Meloy Elmegreen

Vassar College, Dept. of Physics & Astronomy, Box 745, Poughkeepsie, NY 12604

elmegreen@vassar.edu

ABSTRACT

Gas-rich disks in the early universe are highly turbulent and have giant star-forming clumps. Models suggest the clumps form by gravitational instabilities, and if they resist disruption by star formation, then they interact, lose angular momentum, and migrate to the center to form a bulge. Here we study the properties of the bulges formed by this mechanism. They are all thick, slowly rotating, and have a high Sersic index, like classical bulges. Their rapid formation should also give them relatively high $\alpha-$element abundances. We consider fourteen low-resolution models and four high-resolution models, three of which have supernova feedback. All models have an active halo, stellar disk, and gaseous disk, three of the models have a pre-existing bulge and three others have a cuspy dark matter halo. All show the same basic result except the one with the highest feedback, in which the clumps are quickly destroyed and the disk thickens too much. The coalescence of massive disk clumps in the center of a galaxy is like a major merger in terms of orbital mixing. It differs by leaving a bulge with no specific dark matter component, unlike the merger of individual galaxies. Normal supernova feedback has little effect because the high turbulent speed in the

gas produces tightly bound clumps. A variety of indirect observations support the model, including clumpy disks with young bulges at high redshift and bulges with relatively little dark matter.

Subject headings: instabilities — stellar dynamics — galaxies: bulges — galaxies: formation — ISM: evolution

1. Introduction

Numerical simulations have shown that gas-rich primordial galaxy disks can fragment into massive clumps that interact gravitationally and migrate to the center where they merge and form a bulge (Noguchi 1999; Immeli et al. 2004ab; Carollo et al. 2007). In a recent model with an initially uniform disk composed of gas and stars and with an active halo (Bournaud, Elmegreen & Elmegreen 2007a, hereafter BEE07), clump formation and interactions trigger a starburst and redistribute the disk into a smooth exponential profile outside the bulge, while clump ejecta and clump tidal tails create a steeper exponential profile in the far outer regions. The earliest stages resemble high-redshift chain galaxies and clump clusters, with kpc-sized, 10^8 $M_\odot$ clumps (Cowie et al. 1995; van den Bergh et al. 1996; Elmegreen et al. 2004; Conselice et al. 2004). The required high gas fractions and disturbed kinematics are observed at high redshifts (Genzel et al. 2006; Förster Schreiber et al. 2006; Weiner, et al. 2006; Daddi et al. 2008; Bournaud et al. 2008). The final stages in the model resemble modern spirals with a bulge and generally a double-exponential (type II) light profile (Freeman 1970; Pohlen et al. 2002). The bulge and thick disk can form at the same time. The bulge mass fraction is realistic for early type galaxies (BEE07), and, if the disk continues to grow, it is realistic for late types too. In the present paper, we explore the detailed properties of bulges that form this way. In a companion paper (Elmegreen, Bournaud, & Elmegreen 2008), we propose that nuclear black holes form along with the bulges by the coalescence of smaller black holes from each clump.

There are two main types of bulges (e.g., Drory & Fisher 2007; see review in Kormendy & Kennicutt 2004). Early-type galaxies tend to have "classical" bulges that are red, old, and high in α/Fe ratio (indicative of rapid formation), and an $n > 2.5$ Sersic profile (Zoccali et al. 2006; Ballero et al. 2007; McWilliam et al. 2007; Lecureur et al. 2007). Their age, metallicity and abundance ratios (Moorthy & Holtzman 2006), luminosity function (Driver et al. 2007) and position in the fundamental plane (Falcón-Barroso et al. 2002; Thomas & Davies 2006; Jablonka et al. 2007; MacArthur et al. 2007) form a continuous sequence with elliptical galaxies. The most massive bulges and spheroids are of this type (MacArthur et al. 2007), and the Milky Way bulge may be also (Rich et al. 2007; Minniti & Zoccali

2007). Their origin could be related to galaxy-galaxy mergers (Hernquist & Barnes 1991) or cosmological gas accretion (Steinmetz & Muller 1995; Xu et al. 2007). Fu et al. (2003) and Zavala et al. (2007) suggest that classical bulges form from pre-galactic halo clusters or halo fragments, respectively, which lose their angular momentum to the halo.

In contrast, late-type galaxies (e.g., later than Sbc - Thomas & Davies 2006) tend to have "pseudo-bulges," which are somewhat blue, span a wide range of ages, and have more disk-like properties, including small-n Sersic profiles (e.g., Debattista et al. 2006; Carollo et al. 2007). They presumably formed by secular evolution in disks, such as vertical instabilities in bars (Combes, & Sanders 1981; van den Bosch 1998; Avila-Reese et al. 2005; Debattista et al. 2006; Athanassoula 2007, 2008), and torque-driven accretion (Pfenniger & Norman 1990; Zhang 1999; see review in Kormendy & Kennicutt 2004). Rapid secular processes in bars might also build bulges that resemble the classical type in some respects (Athanassoula & Martinez-Valpuesta 2007).

The Noguchi model of bulge formation by disk clump coalescence does not fit either bulge type in standard models. Classical bulges supposedly formed early without significant disks and then accreted their disks later (see review in Conselice 2007). This idea is reinforced by the lack of a correlation between the luminosities of bulges and disks (Balcells et al. 2007). The Noguchi model, although fast enough to form a classical bulge in 1 Gyr, requires a disk first to get the material that coalesces. A pseudo-bulge has a disk first, but the bulge forms by a different mechanism, usually involving bars, and it forms over a much longer time than in the Noguchi model.

The Noguchi model fares better in the context of galactic structure observed at high redshift. The disk clumps that are supposed to coalesce to make a bulge are actually observed in galaxies in the Hubble Space Telescope Ultra Deep Field (HST UDF) and other deep fields out to $z \sim 6$ (Elmegreen et al. 2007a). These clumps are large (> 1 kpc), massive ($\sim 10^8$ $M_\odot$), and young (~ 300 Myr, or ~ 10 internal dynamical times), making them look like scaled-up star complexes formed by common gravitational instabilities (Elmegreen & Elmegreen 2005; Elmegreen, et al. 2007b). They also contribute strongly to the gravitational forces in the disk. If they resist disruption from supernova explosions, then they should migrate to the center and merge in only a few rotations, which is several $\times 10^8$ yrs. The dynamical effect should be analogous to that in a major merger, with a thorough redistribution of orbits and a starburst in the gas (BEE07). In this sense, internal clump coalescence in the Noguchi model is like galaxy coalescence in the classical bulge formation model. Both processes also get less important over time: bulge formation by galaxy mergers becomes less important because the galaxy merger rate decreases; bulge formation by clump mergers becomes less important because the disks become less clumpy. Disk clumps pre-

sumably result from gravitational instabilities, so their mass depends on the turbulent Jeans mass. As turbulent speeds decrease relative to the rotation speed, clump masses decrease relative to the galaxy mass; then their interactions and migrations toward the bulge becomes less severe. An important difference between the two cases is that in galaxy mergers, each component has its own dark matter, whereas in clump mergers, the components are pure baryons.

A strong constraint on the origin of small bulges in massive galaxies was recently discovered by Weinzirl et al. (2008), who found too high a fraction of these bulges compared to the predictions of cosmological simulations. If a bulge is made by a major merger, as in the classical description, then the merger had to occur at a redshift $z > 2$ in order for the galaxy to have had enough time to accrete its massive disk around the merger-remnant bulge. However, the fraction of galaxies with major mergers only at $z > 2$ is much smaller than the fraction of galaxies with small bulges. Thus another origin for small bulges in massive galaxies is required. Weinzirl et al. suggested minor mergers or secular processes are involved. The Noguchi model discussed here is one possible secular process. Considering the prevalence of the right initial conditions for this model in deep galaxy surveys, i.e., highly turbulent and clumpy disks, it may be the primary secular process to form classical-type bulges.

Genzel et al. (2008) propose that bulges and exponential profiles form rapidly in young disks following dynamical evolution. They base this on high resolution observations of Hα and [NII] in $z = 2$ galaxies that show highly turbulent motions in star-forming regions and inner disk masses proportional to age. Elmegreen et al. (2008) similarly find an age and bulge-mass sequence in the clumpy galaxies of the Hubble Space Telescope Ultra Deep Field. The most clumpy types of disks have younger and smaller bulges relative to their star formation clumps than the smoother spirals. Elmegreen et al. suggested that clump cluster and chain galaxies form bulges and thick inner disks while they are still in their highly turbulent stage. When the gas settles, the clumps get smaller, the disk gets smoother, and bulge formation slows down to make a normal spiral.

In the following sections, we first review the observations of high redshift clumpy galaxies and show examples with and without bulges (Sect. 2). Then we present simulations of gas-rich disks that form massive star complexes and follow the evolution of those complexes as they move inward by mutual gravitational interactions (Sect. 3). The properties of the resulting bulges are discussed in Section 4. The effect of supernova feedback on the evolution and coalescence of giant clumps is studied in Section 5. The effect of clump migration on dark matter cusps is discussed in Section 6. Observations that support this model of bulge formation are reviewed in Section 7. Section 8 contains a summary.

2. Observations of High-Redshift Clumpy Disks

Deep HST images with the Advanced Camera for Surveys (ACS) show two types of high redshift galaxies that are clumpy and without bulges or exponential disks: clump-clusters, which are oval collections of bright clumps, discovered by van den Bergh et al. (1996) in the Hubble Deep Field, and chains, which are linear collections of clumps, discovered by Cowie et al. (1995) in HST images of the Hawaii Survey Fields. These two types have similar luminosities and colors, similar clump luminosities and colors, and they collectively have a distribution with respect to their ratio of axes that is constant, as would be the case for circular disks viewed in random orientations (Elmegreen, et al. 2004; Elmegreen & Elmegreen 2005). Thus we suggested that most clump clusters and chains are members of the same population of highly-clumped disk galaxies, viewed at different orientations (Elmegreen, et al. 2005a; see also Reshetnikov, Dettmar, & Combes 2003). Not all clump clusters are single galaxy disks. A few are composed of features with discrepant redshifts so they are probably line-of-sight alignments, and a few others look more like separate galaxies in the process of assembly (see Fig. 5 in Elmegreen et al. 2007b, and Conselice et al. 2008). This is why we prefer to use the general morphological nomenclature of clump-clusters, rather than clumpy galaxies. van den Bergh (2002) called them protospirals, and Conselice et al. (2004) included clump clusters among his more general class of "luminous diffuse objects." For 178 clump clusters in the UDF, $27 \pm 14\%$ of the i_{775} light is in clumps, compared to $\sim 8\%$ for spirals (Elmegreen et al. 2005b). For ten extreme cases, 40% of the i_{775}-band light and 19% of the mass is in clumps (Elmegreen & Elmegreen 2005).

The ACS morphology of clumpy galaxies is based on their far-uv restframe properties, which are dominated by star formation. Rest-frame images in B-band or redder are required to see bulges. In Elmegreen et al. (2007a), we compared i_{775} and NICMOS J images to show weak or no bulges in three clump cluster galaxies, UDF 1666 at redshift $z = 1.318$, UDF 3483 at $z = 1.80$ (photometric), and UDF 6462 at $z = 1.57$, and in one chain galaxy, UDF 7269 at $z = 0.69$ (photometric). Similar comparisons were made in Elmegreen et al. (2008) where the relative bulge masses were also studied. In this latter paper, $\sim 50\%$ of clump clusters and 30% of chain galaxies in the UDF, taken from a sample of galaxies larger than 0.3 arcsec, were observed to have bulges in the H-band NICMOS images. This leaves more than half of the clumpy, high-redshift galaxies without bulges.

Different examples of clumpy galaxies with strong and weak bulges are shown in Figure 1. Each row consists of two galaxies with ACS V-band images on the left and NICMOS H-band images on the right. The top left is UDF 6922 ($z_{phot} = 1.35$), the top right is UDF 4253 ($z_{phot} = 1.04$), the lower left is UDF 7269 ($z_{phot} = 0.69$), and the lower right is UDF 6486 ($z_{phot} = 2.64$). The two top galaxies have central bright concentrations in H-band that are not

evident in the V-band, which shows primarily off-center clumps. These two presumably have bulges. The two in the bottom row have no dominant central concentrations in NICMOS. Other images of clumpy galaxies with and without bulges are shown in Elmegreen et al. (2008).

The identification of bulges in NICMOS images is difficult because the angular resolution is 3 times worse than in ACS images. The best we can say until higher resolution IR observations are available is that among 292 clump cluster and chain galaxies with no evident bulges in the ACS image of the UDF, about half can be examined with NICMOS (because they are large enough or in the NICMOS field of view) and among these, about half contain no obvious central bulges even in NICMOS. These galaxies span redshifts up to ~ 5 in the UDF and are therefore plausible examples of the type of pre-bulge clumpy disks discussed in this paper.

It seems reasonable to assume that some high-redshift clumpy galaxies are fragmented, gas-rich disks. The clumps probably formed by gaseous gravitational instabilities, as in local galaxies, in which case the turbulent speed should be moderately large compared to the rotation speed, perhaps several tens of percent. This makes the clump size large compared to the galaxy radius, so there are only a few giant clumps in each galaxy. The high turbulence is in agreement with observations by Genzel et al. (2006), Förster Schreiber et al.(2006), and others referenced above. One of the clump-clusters that has a small bulge or reddish stellar region, UDF 6462, has a global rotation curve indicative of a single galaxy with highly disturbed velocities at the positions of the clumps, suggesting both high turbulence and non-circular motions (Bournaud et al. 2008). The bulge in UDF 6462 is redder than the clumps, somewhat centralized, and has a higher metallicity than the rest of the disk.

3. Numerical simulations

The most relevant observations for a model of clumpy galaxies are the overall galaxy size, and the clump masses, separations and numbers. If the clumps form by gravitational instabilities in the gaseous component of an irregular disk, then their properties depend on local values of the turbulent speed σ and column density Σ. To get a small number of massive clumps, we need a relatively high ratio of turbulent speed to rotation speed, $\sim 10\%$ or more, and to get such a turbulent disk gravitationally unstable so that it forms clumps, we need a fairly high gas column density, which means a high gas-to-star ratio in the disk at that time. Many other details of the initial conditions are less important for this bulge formation model. The clumps should have a mass comparable to the disk Jeans mass, which is $M_J \sim \sigma_{gas}^4/\left(G^2\Sigma\right)$, and they should have a separation comparable to the Jeans length,

$L_J \sim 2\sigma_{gas}^2/(G\Sigma)$. If the dispersion for gas is large, comparable to that for the disk stars, then Σ in this equation will have a strong contribution from disk stars, i.e., both stars and gas can contribute to the clump. When the Jeans length is a large fraction of the disk scale length, the clump masses will be a large fraction of the disk mass, and such clumps will interact strongly (BEE07). Cosmological simulations have more realism than our models on extragalactic scales, but they are not generally tuned to give clumpy disks like those we see at intermediate to high redshifts. Analytical models that approximate disk accretion with viscosity and consider thermal cooling (e.g., Lodato & Natarajan 2006) are also not as useful as direct simulations for following the complexity of turbulent disk fragmentation and evolution.

The evolution of gas-rich galaxy disks is modeled here in the same manner as in BEE07. We use a particle-mesh sticky-particle code (see Bournaud & Combes 2002, 2003). Sticky-particle parameters are $\beta_r = \beta_t = 0.7$ for all but run 4, which has $\beta_r = \beta_t = 0.8$. Star formation follows a local Schmidt law where the probability per timestep that each gas particle is transformed into a stellar particle is proportional to the local gas density to the power 1.4 (e.g., Kennicutt 1998). The proportionality factor gives a star formation rate of 3.5 $M_\odot$ yr^{-1} in the initially uniform disk.

In all our models, the initial disk is composed of gas and stars with a uniform surface density (i.e., chain and clump cluster galaxies do not have exponential disks; Elmegreen et al. 2005b). The initial disk radius is 6 kpc and the thickness is $h = 700$ pc with a $\mathrm{sech}^2(z/h)$ vertical distribution. The disk mass (stars+gas) is 7×10^{10} $M_\odot$. Stars have a Toomre parameter in the stable regime, $Q_s = 1.5$, but the mixed disk of stars and gas is unstable.

We first analyze a series of 14 low-resolution runs with a grid resolution and gravitational softening length of 110 pc. Stars, gas, and dark matter halo are modeled with one million particles each in these runs. Feedback from star formation is not included. Runs 0 to 7 are the same as in BEE07, and their initial parameters were summarized in Table 1 of BEE07. The main fixed parameters were recalled above. The gas mass fraction in the disk, f_G, is 0.5 except for runs 4 and 5, where it is 0.25 and 0.75. The halo-to-disk mass ratio, H/D, inside the initial disk radius, is 0.5 except for runs 6 and 7, where it is 0.25 and 0.80.

Runs 0 to 7 have no initial bulge and a dark halo that is a Plummer sphere with a scale-length of 15 kpc. In addition, runs 0N, 1N, 2N have a ΛCDM cuspy halo (Navarro, Frenk & White 1997) with a cusp scale-length $r_S = 6$ kpc (concentration parameter 16.7 for a virial radius of 100 kpc). The other parameters including the gas fractions and halo-to-disk mass ratios are unchanged from runs 0, 1 and 2, respectively. Runs 0B, 1B, 2B are like runs 0, 1, and 2, but they have a small initial bulge that is a Plummer sphere with 10% of the

disk mass and a radial scale-length of 600 pc.

We also performed higher-resolution models, with some including supernova feedback. The number of particles of each type was larger by a factor 3, the grid resolution and softening length were improved by a factor 2 in each direction everywhere, and they were improved by a factor 4 at radii smaller than 4 kpc. Clump coalescence occurs in this inner region, so the high resolution cases, where the spatial resolution is 28 pc, consider this process best.

With high resolution, Run HR-0 has an initial gas fraction of 60%, an initial bulge of 4% of the disk, and the other parameters as in the fiducial Run 0. Runs HR-0-F1, HR-0-F2 and HR-0-F3 have the same initial conditions and resolution as run HR-0, but with supernova feedback included. We used the feedback model proposed by Mihos & Hernquist (1994). A supernova is assumed to occur for each 50 $M_\odot$ of stars formed. A fraction ϵ of the 10^{51} erg energy of each supernova is released in the form of radial velocity kicks applied to gas particles within the closest cells. We used $\epsilon = 2 \times 10^{-4}$ in run HR-0-F1 (which is about the value suggested by Mihos & Hernquist 1994), $\epsilon = 10^{-3}$ in run HR-0-F2 and $\epsilon = 10^{-2}$ in run HR-0-F3.

During the course of each simulation, clumps were identified every 25 Myr as regions where the surface density is locally larger than the radial average by a factor of 3. Only clumps with masses larger than 2×10^8 $M_\odot$ and sizes smaller than 3 kpc were considered: this size limitation avoids spiral arms (see BEE07). Sub-structures like OB associations and small dense clusters are expected to form inside the main clumps of real galaxies, but we cannot resolve this in the simulations.

4. Bulge Properties

Properties of the bulges formed in the low and high resolution runs without feedback are first considered. The influence of supernovae (SNe) in runs HR-0-F1 to HR-0-F3 will be discussed in section 5. The time-dependent mass column density in the fiducial run 0 was shown in Figure 4 of our previous paper, BEE07. Giant stellar clumps formed in the gas-rich initial disk and then migrated to the center where they made a bulge. About half the clump mass was left in the disk and the other half got to the center. An exponential disk formed outside.

Figures 2 and 3 show the new fiducial runs, 0N, with an initial NFW halo, and 0B, with an initial central bulge. The timescale for clump merging has increased slightly in both cases compared to run 0 because of the relatively smaller mutual forces between the clumps: smaller compared to the dark matter force in run 0N and smaller compared to the combined

disk+bulge force in run 0B. The evolution of the high resolution run HR-0 is shown on the top in Figures 6 and 7.

4.1. Bulge mass

The fractional clump masses, f_C, bulge masses, and bulge-to-total (baryonic) mass fractions after 1 Gyr are given in Table 1. Runs 0 to 7 and HR-0 have bulge fractions ranging from 0.12 to 0.36 (average 0.24). Runs with a cuspy dark matter halo have about the same final bulge mass fractions as those with a Plummer sphere halo. Runs with an initial 10% bulge have slightly larger final bulge masses than those without an initial bulge. This increase is not the full 10% because increased tidal forces near the center disrupt the clumps earlier before they coalesce. Bulge growth is somewhat regulated in this way. This keeps the final bulge-to-disk ratio compatible with that in present-day early-type spirals, even when a primordial bulge is present from an earlier clump-cluster phase or another formation process.

4.2. Bulge Density Profile

Figure 4 shows radial disk column density profiles, ($\Sigma(r)$, normalized to the central value) of the bulge regions up to $\sim$ 1.5 kpc, where the disks become exponential. We plot $\log[-\log(\Sigma)]$ versus $\log(r)$ because that has a constant slope of $1/n$ in a Sersic profile with projected normalized column density $\Sigma = \exp[-(r/r_0)^{1/n}]$. The model bulges have steep Sersic indices, with an average of $n \simeq 4$ (between 3 and 4.5) in the 100–500 pc radial range. The Sersic index decreases at radii of 500 to 1000 pc. The bulge in the higher-resolution run HR-0 also has a Sersic index clearly larger than 2 and close to 4 for $r < 500$ pc; the best fit in the 100-500 pc range is $n = 3.4$. Thus the model produces central concentrations with the morphology of classical bulges.

4.3. Bulge Kinematics

The bulges formed by clump coalescence are not fast rotators. Figure 5 shows the line-of-sight velocity (V) and velocity dispersion (σ_{bulge}) for the fiducial run 0 at the final stage, considering two orthogonal edge-on projections. The bulge central velocity dispersion was measured as follows: for each model, we built 50 independent 2-D projections of the stellar content, uniformly distributed over the sine of the inclination to represent an average over all possible viewing angles. The line-of-sight velocity dispersion was computed inside

a projected aperture diameter of 110 pc (the grid resolution), and for each model we kept the average value over all projections. We do not attempt to subtract the disk component from edge-on projections, nor to make a direct 3-D measurement, because this would not be done in observations. Measuring the mass-weighted line-of-sight dispersion within a larger projected aperture of 500 pc, we find values between 7% higher and 11% lower than the measurement in the central 110 pc. Thus the projected radial gradient in the dispersion is relatively small in the bulge. This result was also found observationally by Gebhardt et al. (2000), who showed that the dispersion gets high only in the very central regions close to a black hole.

Figure 5 indicates that the bulge region has a strong increase in the velocity dispersion compared to the disk. While the V/σ_{bulge} ratio in the exponential disk exceeds 2, the luminosity-weighted average value in the central 750 pc, which contains two-thirds of the bulge mass (green circles on Fig. 5), is much smaller, between 0.4 and 0.5 for the two projections. This is actually an upper limit to V/σ_{bulge} in the bulge because of unavoidable disk contamination. In this respect, clump mergers that form bulges are like galaxy mergers that form elliptical galaxies. Both provoke a large kinematical heating that forms a spheroid dominated by random motions. Clump mergers are not like the in-spiral of small dense clusters from dynamical friction, which can leave a rapidly rotating core. Values of the bulge line-of-sight velocity dispersion for all simulations are in Table 1. The average is 130 km s^{-1}.

The bulge velocity dispersion was not affected by resolution. Even at higher resolution, the bulges are slowly rotating and have high velocity dispersions. The bulge morphology and kinematics in model HR-0 are shown in Figure 8. This bulge is rotating with $V \leq 60$ km s^{-1}, and it has a velocity dispersion $\sigma \geq 80$ km s^{-1} within its half-mass radius.

All of the bulges are somewhat flattened in both the high and low resolution runs. This flattening results from a combination of slight bulge rotation, anisotropic velocity dispersion, and a flattened disk potential.

5. Effects of Supernova Feedback on the Evolution of High-Redshift Clumpy Galaxies

The models described so far and in BEE07 include star formation but no SN feedback. The concern is whether energy injected by SNe can disrupt the clumps before they reach the center. Immeli et al. (2004a,b) had feedback in their models and the clumps were not disrupted, however their clump masses were larger than in the observations and in our models. Here we consider three high-resolution models, HR-0-F1, HR-0-F2, and HR-0-F3,

that have different fractions ϵ of SN energy re-injected into the local gas kinetic energy ($\epsilon = 2 \times 10^{-4}$, 10^{-3}, and 10^{-2}, respectively). The evolution of these models is shown in the bottom three rows of Figures 6 and 7.

According to Mihos & Hernquist (1994), realistic values for ϵ in kinetic feedback models should be around 2×10^{-4} (our run HR-0-F1) and not higher than 10^{-3} (our run HR-0-F2). These two runs have long-lived, massive clumps of gas and stars in their disks that survive until they coalesce into the central bulge (Figs. 6 and 7). Only the lowest mass clumps (10^7 $M_\odot$) are significantly reduced by feedback. As measured in Table 1, the masses of the largest clumps are only slightly reduced when feedback is added, and as a result the bulge growth is reduced too, both by about 10%. This is a rather small effect, so feedback is not the main driver of clump disruption. As shown in BEE07, clumps typically release half of their mass into the disk before they reach the bulge because of tidal forces and shear. This keeps the final bulge-to-disk mass ratio rather low. In our models HR-0-F1 and HR-0-F2, SN feedback further regulates the bulge growth in a modest way, but the cores of the clumps clearly survive until they reach the central kpc and coalesce into the bulge.

The edge-on view of the gas disk in run HR-0-F2 ($\epsilon = 10^{-3}$; Fig. 7) shows that it is significantly thickened. At the mid-course of the simulation, the gas layer has an average scale-height of 1.6 kpc, larger than the initial conditions and thicker than the star-forming layers in chain galaxies (Elmegreen & Elmegreen 2006). This model should then be taken as an upper limit on the feedback efficiency, in agreement with what Mihos & Hernquist inferred at lower redshift. Even in this case, though, the cores of the massive clumps survive until they reach the central bulge. If we increase even more the feedback efficiency (run HR-0-F3), the clumps become short-lived: they form in the gas but are rapidly disrupted, with no visible counterpart remaining in the stellar mass. In this case no bulge formation by clump coalescence can occur. The gas disk is also nearly destroyed in this case: the thickening is so large that the gas disk resembles a spheroid and even the stellar disk thickens over time.

It is thus unlikely that supernova feedback can disrupt 10^8 $M_\odot$ clumps in high-redshift galaxies; otherwise the gas disk itself would get dispersed. Assuming a lower feedback efficiency but a higher star formation efficiency, or a higher supernova fraction in the IMF, would lead to the same conclusion. If the energy input from stellar feedback is low enough to preserve the gas disk, then the most massive clumps that form are likely to survive for a few disk rotations and reach the center. Supernovae feedback should be more important in lower-mass galaxies, which should have lower gas turbulent speeds and easier clump disruption. This could explain why lower mass galaxies (i.e., later Hubble types) tend to have lower bulge-to-disk mass ratios.

6. Evolution of the Dark Matter Cusp

Three of the models have a cuspy initial dark matter halo, following Navarro et al. (1997). The evolution of the disk does not depend much on this cusp, as shown above, but the evolution of the cusp depends a little on the disk. Figure 9 shows the halo density profiles before and after these three simulations. A control run with a rigid disk potential is also shown (dotted line). When the disk can evolve through the formation and interaction of clumps, the central cusp becomes considerably weaker, amounting to a factor of ~ 3 in central halo density. The cusp scale-length increases also. This change is a result of halo heating by the moving massive clumps when they reach the center. The central cusps do not go away, but they get reduced. Their reduction should be greater in lower mass galaxies if the disk Jeans mass is about the same (i.e., if the gas velocity dispersion and column density are about the same for a smaller mass galaxy). The reduction should be greater also if several episodes of gas accretion, clump formation and bulge growth take place during the life of a galaxy. Each episode would erode the cusp a little more.

7. Discussion

Numerical simulations suggest that primitive gas-rich disks should fragment into clumpy star-formation complexes with masses of $\sim 10^8\ M_\odot$ or more, and that these complexes should interact gravitationally and move to the galaxy center where they combine to form a bulge. The surrounding disk becomes exponential in the process. There are many assumptions here, the simulations are highly idealized, and the initial galaxies are not fully cosmological with realistic gas accretion and hierarchical build-up. Still, the most important aspects of the model are rather fundamental: young galaxies are gas-rich, gravitational instabilities are inevitable (as in modern galaxies), and clump interactions follow from the relatively large Jeans masses. Our models also suggest that the most massive clumps can survive star-formation feedback during the time it takes them to coalesce. Thus, we are led to ask whether this bulge formation scenario is compatible with the properties of real galaxies and if there is either direct or indirect evidence for it.

First, we have illustrated the kinds of young galaxies where these processes should operate: the clump cluster and chain galaxies with weak or no bulges that are seen out to the detection limit at $z \sim 5$ in all high-resolution deep images (Sect. 1, 2). The observed clump masses, sizes, positions, numbers, and ages in these galaxies are reproduced by the models without fine tuning. The key ingredient is a ratio of velocity dispersion to rotation speed that is several times larger than in local galaxies: this large dispersion makes the interstellar Jeans mass equal to the observed clump mass for star formation that is triggered

by gravitational instabilities (e.g., Elmegreen et al. 2007b). Such large dispersions are observed in high redshift disks (Sect. 1).

Sargent et al. (2007) also note that the co-moving density of bulge-free disks among intermediate-size galaxies increases out to $z = 1$, while the co-moving density of classical bulgy disks (as determined from their high-n Sersic profiles) decreases, keeping the total disk comoving density about the same. They conclude that at least some high-n bulges have formed by secular disk processes since $z = 1$. Balcells & Domínguez-Palmero (2007) find a similar coeval evolution of classical bulges and disks: bulge colors correlate with disk colors and red bulges are rarely surrounded by purely blue disks in the redshift range from 0.1 to 1.2. Thus there is good evidence for bulge-free disks at high redshift, and for a transition from bulge-free to classical-bulge galaxies over time. This is compatible with the standard model of bulge formation in galaxy mergers, and also with our model of bulge formation by baryonic clump mergers.

The simulations show that the bulges formed this way have properties typical of classical, early-type galaxy bulges. They are slow rotators with high velocity dispersions, thick perpendicular dimensions, and high Sersic indexes. The model timescale from the formation of giant clumps to their merging in the bulge is about 1 Gyr, consistent with the evidence summarized in Section 1 for rapid formation of classical bulges, including that in the Milky Way (e.g., Lecureur et al. 2007) and $z \sim 2$ galaxies (Genzel et al. 2008; Elmegreen et al. 2008). Longer bulge formation timescales are possible if the clump formation phase in the disk is prolonged, as might be the case with continued cosmological gas accretion.

The merger of disk clumps is somewhat similar to the merger of small galaxies. The initial angular momentum of the clumps is lost to the disk and halo, so all that remains after their merger is a spheroidal bulge supported mainly by velocity dispersions. An important difference between bulge formation by clump mergers and bulge formation by galaxy mergers concerns the dark matter content of the merging entities. Disk clumps, forming by disk instabilities, contain no halo dark matter from the surrounding galaxy, and so the bulges they form contain no additional dark matter either. In contrast, galaxy mergers bring in considerable amounts of dark matter with them, and much of this should end up in the bulge or spheroid (e.g. Dekel et al. 2005). The amount of bulge dark matter depends on how many bulge stars form at the time of the merger: merger-driven gas accretion followed by star formation to make a bulge brings in relatively little dark matter, whereas merging warm stellar populations should preserve their initial dark matter content. Because observations of early-type galaxy bulges show relatively little dark matter (Corradi & Capaccioli 1990, Noordermeer et al. 2007, Corsini 2007), the galaxy merger model of bulge formation could have more difficulty than the clump merger model in this respect.

Another test of our model involves dark matter cusps (Navarro et al. 1997). Dark matter in merging galaxies adds to the cusp during hierarchical buildup, while massive baryonic clumps that stir the central regions reduce these cusps by increasing the central dark matter velocity dispersion (see also El-Zant, Shlosman, & Hoffman 2001; Sect. 6). Neither of these two bulge-forming mechanisms can completely remove the cusps. Either real galaxies never had cusps, or their cusps have been washed out by various dynamical mechanisms. The merging of disk clumps into a bulge eases the cusp problem, while the merging of cusp-containing galaxies makes the problem worse.

The case for classical bulge formation by galaxy coalescence has been weakened also by the observation that early-type bulges may have smaller Sersic n than previously thought. Carollo, Stiavelli, & Mack (1998) found nuclear star clusters in half of the 75 galaxies they observed with HST, spanning a wide range of Hubble types, and noted that many had exponential profiles outside the clusters and few had pure $n = 4$ Sersic profiles. Balcells et al. (2003) also found for early-type galaxies (S0-Sbc) that nuclear star clusters, which are usually unresolved from the ground, convert low-n profiles into high-n profiles artificially. High-n profiles can be explained by major mergers and violent relaxation (van Albada 1982; Barnes 1988; Bournaud et al. 2005, Naab & Trujillo 2006) or by numerous minor mergers (Bournaud et al. 2007b), but if the profiles have lower n, then the merger scenario is less compelling. Our models form high-n bulges by clump mergers and are subject to the same criticism. If all bulges have low n except for unresolved nuclear clusters, then our model cannot explain them – or strong supernova feedback is required to decrease the mass concentration. More high-resolution bulge profiles are required for this important test.

In the case of late-type or low-mass bulges, which are mostly pseudo-bulges, there is considerable evidence that they come from disks, including correlations between bulge colors and scale lengths and disk colors and scale lengths (MacArthur et al. 2003; Carollo et al. 2001; 2007; see Kormendy & Kennicutt 2004). The implied processes usually involve torque-driven inflows and vertical resonances from bars and spirals. Our models differ from this in that they are fast and require a more primitive disk, one dominated by turbulent gas and little pre-existing bulge, bar, or spiral potentials. A predominantly stellar disk with a bar already, or with enough of a stellar mass to generate strong spiral torques, is not as likely as a primitive disk to fragment into giant clumps that interact gravitationally and merge in the center. We showed in Section 4.1 that an initial bulge increases the tidal force on the clumps and limits the mass they can deliver to the center.

8. Conclusions

Gas-rich disks with relatively high turbulent speeds should fragment into massive, star-forming clumps and quickly evolve to resemble the chain and clump-cluster galaxies observed at high redshift. Further evolution should lead to clump coalescence and the overall structure of early-type disk galaxies, with smooth (Type II) exponential profiles and Sersic $n \sim 4$ bulges. The bulge and inner thick disk stars form fast enough to become enriched with α elements, as required, and their velocity dispersions are realistically large. Direct observations in support of this model include clumpy, highly-turbulent disks and the presence of relatively young, low-mass bulges at intermediate to high redshifts (Sects. 1, 2). Indirect observations include a gradual transition in the classical bulge fraction in disks from redshift $z \sim 1$ to 0 (Sect. 7), a high fraction of massive galaxies with relatively low-mass bulges (Sect. 1), and a lack of dark matter specific to the bulge component (Sect. 7), all of which constrain bulge formation by major mergers of individual galaxies. We also note some tendency for clump interactions to heat a dark matter cusp if there is one, and in our simulations, this lowers the cusp density by a factor of ~ 3. More simulations will be required to determine if multiple bulge-building episodes continue to reduce the cusp density.

The primary two motivations to consider bulge formation by this mechanism are the large turbulent speeds and the extremely clumpy structures observed in high redshift galaxies. Gravitational instabilities in highly turbulent disks will form stars in extremely massive clumps, so the two observations go together. The present simulations start at this point and show that such clumps will interact strongly with the disk stars and with each other and, as a result, lose angular momentum and migrate to the center. Bulge formation follows. Our simulations with supernova feedback indicate that the massive clumps survive long enough for this whole process to occur, even if feedback regulates bulge growth slightly. The models also indicate that clump coalescence is a lot like galaxy coalescence in that the final bulges formed by these two mechanisms have similar velocity dispersions, rotations, light profiles, and three-dimensional structures. Bulge formation by clump coalescence is expected to get less frequent over time as disk turbulence subsides, because the star-forming clumps will get less massive with the lower turbulent speeds. This decrease in bulge formation by clump coalescence parallels the decrease expected for bulge formation by galaxy coalescence.

The dynamical processes shown here are fundamental yet rapid, suggesting they may be present but unrecognized in other published simulations, including large-scale cosmological simulations that have enough resolution to see structure in disk galaxies (e.g., Rasera & Teyssier 2006; Ocvirk et al. 2008). If the clumpy-disk, bulge-formation phase lasts for only a few disk rotations, and most of the time in a simulation consists of calm secular phases alternating with minor and major mergers, then this important first step in the formation of a

galaxy might be missed compared to the subsequent longer-term evolution. The contribution of such clumpy phases to the star formation history might be overlooked too. Still, the processes described here should be present in simulations with enough resolution.

Numerical simulations were carried out on the NEC-SX8R vector computer at CEA/CCRT. D.M.E. thanks Vassar College for publication support. Helpful comments by the referee are gratefully acknowledged.

REFERENCES

Athanassoula, E. 2007, in Island Universes, Astrophysics and Space Science Proceedings, Springer, p. 195

Athanassoula, E., & Martinez-Valpuesta, I. 2007, astroph/0710.1518

Athanassoula, E. 2008, astroph/0802.0155

Avila-Reese, V., Carrillo, A., Valenzuela, O., & Klypin, A. 2005, MNRAS, 361, 997

Balcells, M., Graham, A.W., Domnguez-Palmero, L., & Peletier, R.F. 2003, ApJ, 582, L79

Balcells, M., Graham, A.W., & Paletier, R.F. 2007, ApJ, 665, 1104

Balcells, M., & Dominguez-Palmero, L. 2007, astroph/0710.0494

Ballero, S. K., Matteucci, F., Origlia, L., & Rich, R. M. 2007, A&A, 467, 123

Barnes, J.H. 1988, 331, 699

Baumgardt, H., & Makino, J. 2003, MNRAS, 340, 227

Bournaud, F., & Combes, F. 2002, A&A, 392, 83

Bournaud, F., & Combes, F. 2003, A&A, 401, 817

Bournaud, F., Jog, C. J., & Combes, F. 2005, A&A, 437, 69

Bournaud, F., Elmegreen, B.G., & Elmegreen, D.M. 2007a, ApJ, 670, 237

Bournaud, F., Jog, C. J., & Combes, F. 2007b, A&A, 476, 1179

Bournaud, F., Daddi, E., Elmegreen, B. G., Elmegreen, D. M. & Elbaz, D. 2008, A&A in press, astroph/0803.3831

Carollo, C. M., Stiavelli, M., & Mack, J. 1998, AJ, 116, 68

Carollo, C. M., Stiavelli, M., de Zeeuw, P. T., Seigar, M., & Dejonghe, H. 2001, ApJ, 546, 216

Carollo, C. M., Scarlata, C., Stiavelli, M., Wyse, R. F. G., & Mayer, L. 2007, ApJ, 658, 960

Combes, F., & Sanders, R.H. 1981, A&A, 96, 164

Conselice, C.J. 2007, astroph/0709.4614

Conselice, C.J., et al. 2004, ApJ, 600, L139

Conselice, C. J., Rajgor, S., & Myers, R. 2008, MNRAS, 386, 909

Corradi, R. L. M., & Capaccioli, M. 1990, A&A, 237, 36

Corsini, E. M. 2007, astroph/0709.3815

Cowie, L.L., Hu, E.M., & Songaila, A. 1995, AJ, 110, 1576

Daddi, E., Dannerbauer, H., Elbaz, D., Dickinson, M., Morrison, G., Stern, D., & Ravindranath, S. 2008, ApJL, 673, 21

Debattista, V.P., Mayer, L., Carollo, C. M., Moore, B., Wadsley, J., & Quinn, T. 2006, ApJ, 645, 209

Dekel, A., Stoehr, F., Mamon, G. A., Cox, T. J., Novak, G. S., & Primack, J. R. 2005, Nature, 437, 707

Dekel, A., & Cox, T. J. 2006, MNRAS, 370, 1445

Dekel, A., & Woo, J. 2003, MNRAS, 344, 1131

Driver, S.P., Allen, P.D., Liske, J., Graham, A.W. 2007, ApJ, 657, L85

Drory, N., & Fisher, D.B. 2007, ApJ, 664, 640

Elmegreen, D.M., Elmegreen, B.G., & Hirst, A.C., 2004, ApJ, 604, L21

Elmegreen, B.G., & Elmegreen, D.M. 2005, ApJ, 627, 632

Elmegreen, B.G., & Elmegreen, D.M. 2006, ApJ, 650, 644

Elmegreen, D.M., Elmegreen, B.G., Rubin, D.S., & Schaffer, M.A. 2005a, ApJ, 631, 85

Elmegreen, B.G., Elmegreen, D.M., Vollbach, D.R., Foster, E.R., & Ferguson, T.E., 2005b, ApJ, 634, 101

Elmegreen, D.M., Elmegreen, B.G., Ravindranath, S., & Coe, D.A., 2007a, ApJ, 658, 763

Elmegreen, D.M., Elmegreen, B.G., Ferguson, T., & Mullan, B. 2007b, ApJ, 663, 734

Elmegreen, B.G., Bournaud, F., & Elmegreen, D.M. 2008, ApJ, in press, arXiv:0805.2266

Elmegreen, D.M., Elmegreen, B.G., Fernandez, X.M., & Lemonias, J.J. 2008, ApJ, submitted

El-Zant, A, Shlosman, I. & Hoffman, Y. 2001, ApJ, 560, 636

Falcón-Barroso, J., Peletier, R.F., & Balcells, M. 2002, MNRAS, 335, 741

Förster Schreiber, N. M., et al. 2006, ApJ, 645, 1062

Freeman, K.C. 1970, ApJ, 160, 811

Fu, Y. N., Huang, J. H., & Deng, Z. G. 2003, MNRAS, 339, 442

Gebhardt, K., et al. 2000, ApJ, 539, L13

Genzel, R., et al. 2006, Nature, 442, 786

Genzel, R., et al. 2008, ApJ, in press, aarXiv:0807.1184

Hernquist, L., & Barnes, J. E. 1991, Nature, 354, 210

Immeli, A., Samland, M., Gerhard, O., & Westera, P. 2004a, A&A, 413, 547

Immeli, A., Samland, M., Westera, P., & Gerhard, O. 2004b, ApJ, 611, 20

Jablonka, P., Gorgas, J., & Goudfrooij, P. 2007, A&A, 474, 763

Kennicutt, R.C., Jr. 1998, ApJ, 498, 541

Kormendy, J., & Kennicutt, R.C., Jr. 2004, ARA&A, 42, 603

Lecureur, A., Hill, V., Zoccali, M., Barbuy, B., Gómez, A., Minniti, D., Ortolani, S., Renzini, A. 2007, A&A, 465, 799

Lodato, G. & Natarajan, P. 2006, MNRAS, 371, 1813

MacArthur, L,A., Courteau, S., & Holtzman, J. A. 2003, ApJ, 582, 689

MacArthur, L.A., Ellis, R.S., Treu, T., U, V., Bundy, K., Moran, S.M. 2007, astroph/0711.0238

McWilliam, A., Matteucci, F., Ballero, S., Rich, R. M., Fulbright, J. P., & Cescutti, G. 2007, astroph/0708.4026

Minniti, D., & Zoccali, M. 2007, astroph/0710.3104

Mihos, J. C., & Hernquist, L. 1994, ApJ, 437, 611

Moorthy, B.K., & Holtzman, J.A. 2006, MNRAS, 371, 583

Naab, T., & Trujillo, I. 2006, MNRAS, 369, 625

Navarro, J.F., Frenk, C.S., & White, S.D.M. 1997, ApJ, 490, 493

Noguchi, M. 1999, ApJ, 514, 77

Noordermeer, E., van der Hulst, J. M., Sancisi, R., Swaters, R. S., & van Albada, T. S. 2007, MNRAS, 376, 1513

Ocvirk, P., Pichon, C., & Teyssier, R. 2008, astro-ph/0803.4506

Pfenniger, D., & Norman, C. 1990, 363, 391

Pohlen, M., Dettmar, R.-J., Lŭtticke, R., & Aronica, G. 2002, A&A, 392, 807

Rasera, Y., & Teyssier, R. 2006, A&A, 445, 1

Reshetnikov, V. P., Dettmar, R.-J., & Combes, F. 2003, A&A, 399, 879

Rich, R. M., Howard, C., Reitzel, D.B., Zhao, H.S., & de Propris, R. 2007, astroph/0710.5162

Sargent, M.T. et al. 2007, ApJS, 172, 434

Steinmetz, M., & Muller, E. 1995, MNRAS, 276, 549

Thomas, D., & Davies, R.L. 2006, MNRAS, 366, 510

van Albada, T.S. 1982, MNRAS, 201, 939

van den Bergh, S. 2002, PASP, 114, 797

van den Bergh, S., Abraham, R.G., Ellis, R.S., Tanvir, N.R., Santiago, B.X., & Glazebrook, K.G. 1996, AJ 112, 359

van den Bosch, F.C. 1998, ApJ, 507, 601

Weiner, B. J., et al. 2006, ApJ, 653, 1027

Weinzirl, T., Jogee, S., Khochfar, S., Burkert, A., & Kormendy, J. 2008, arXiv:0807.0040

Xu, B.-X., Wu, X.-B., & Zhao, H.-S. 2007, ApJ, 664, 198

Zavala, J., Okamoto, T., Frenk, C.S. 2007, astroph/0710.2901

Zhang, X. 1999, ApJ, 518, 613

Zoccali, M., Lecureur, A., Barbuy, B., Hill, V., Renzini, A., Minniti, D., Momany, Y., Gómez, A., & Ortolani, S. 2006, A&A, 475, L1

Table 1: Masses, Mass fractions, and Bulge Velocity Dispersions

Run ID	f_C	Bulge Mass $\times 10^9\ M_\odot$	Bulge/Total Mass Ratio	σ_{bulge} km s^{-1}
0	0.38	21	0.30	121
1	0.32	14.7	0.21	117
2	0.31	13.3	0.19	108
3	0.39	23.1	0.33	146
4	0.26	9.8	0.14	87
5	0.34	22.4	0.32	184
6	0.41	25.2	0.36	178
7	0.23	8.4	0.12	91
0N	0.33	19.6	0.28	163
1N	0.29	12.6	0.18	118
2N	0.32	14.7	0.21	122
0B	0.31	24.6	0.32	145
1B	0.26	20.8	0.27	125
2B	0.28	19.3	0.25	109
HR-0	0.36	19	0.26	123
HR-0-F1	0.33	18	0.25	119
HR-0-F2	0.30	14	0.20	107

Note. — 1. Run ID. Runs with N start with a NFW halo profile, runs with B start with an initial bulge.
2. Mass fraction in clumps at the time of peak clumpiness.
3. Bulge mass (measured as in BEE07).
4. Final bulge-to-total mass ratio, not including dark matter in the total.
5. Bulge central line-of-sight velocity dispersion averaged from 50 projections uniformly distributed over the sine of the inclination angle.

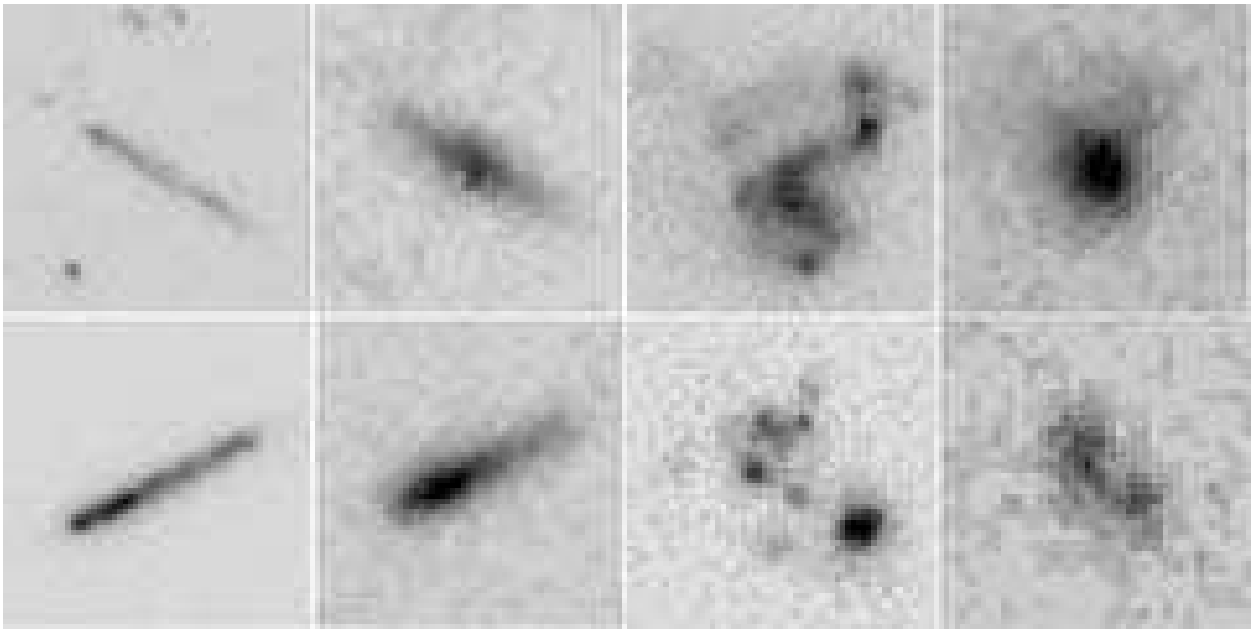

Fig. 1.— Two clumpy galaxies with strong bulges (top) and two with weak or no bulges (bottom). For each image pair, ACS V-band images are on the left and NICMOS H-band images (at 3×worse resolution) are on the right. Top left: UDF 6922 ($z_{phot} = 1.35$), top right: UDF 4253 ($z_{phot} = 1.04$), lower left: UDF 7269 ($z_{phot} = 0.69$), lower right: UDF 6486 ($z_{phot} = 2.64$). Galaxies in the top row have central bright concentrations in H-band that are not evident in the V-band, which shows primarily off-center clumps. Galaxies in the bottom row do not have bright central concentrations in NICMOS. Four other examples are in Elmegreen et al. (2007a) and a systematic study of bulgeless clumpy disks is in Elmegreen et al. (2008). [Image degraded for astro-ph]

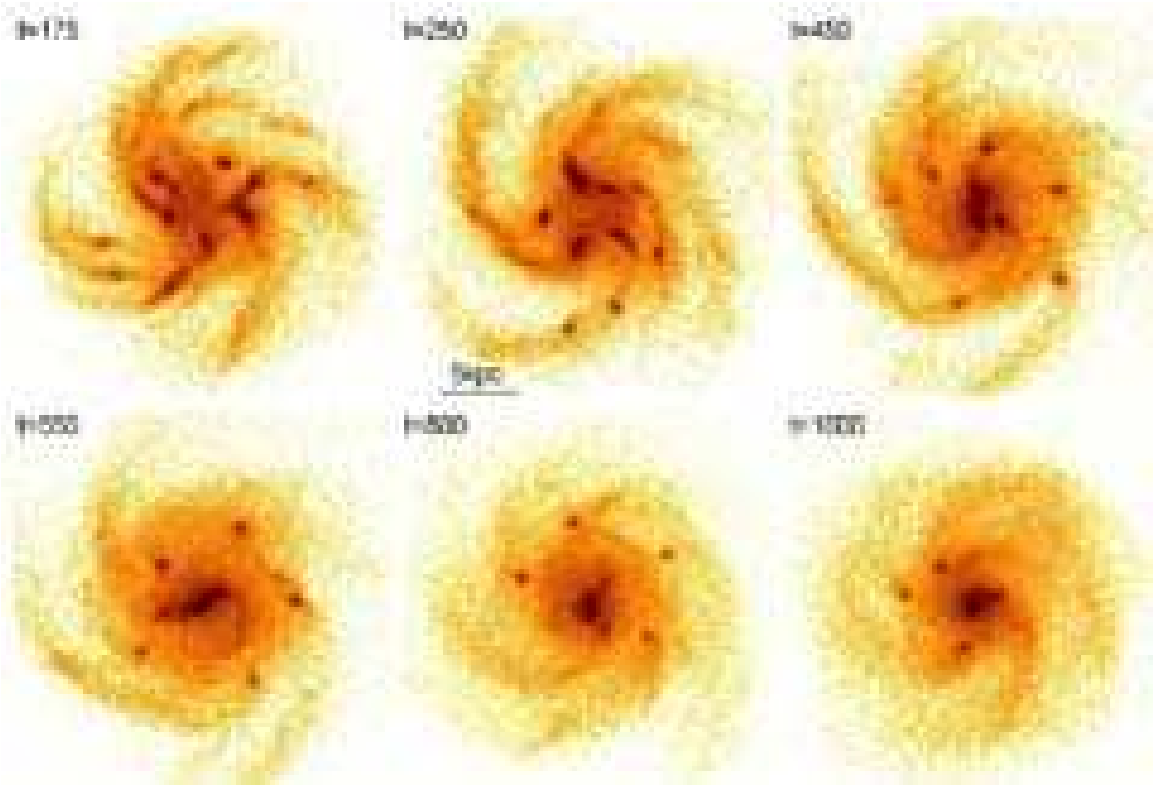

Fig. 2.— Face-on snapshots of the disk mass density (gas and stars) for run 0N, which has a cuspy dark matter profile. Time is in Myr. Clumps form quickly in the disk and move to the center, where they coalesce into a bulge within 1 Gyr. Extra star formation in the bulge region is triggered at the time of merging too. A few clumps remain in the disk when the simulation ends. [Image degraded for astro-ph]

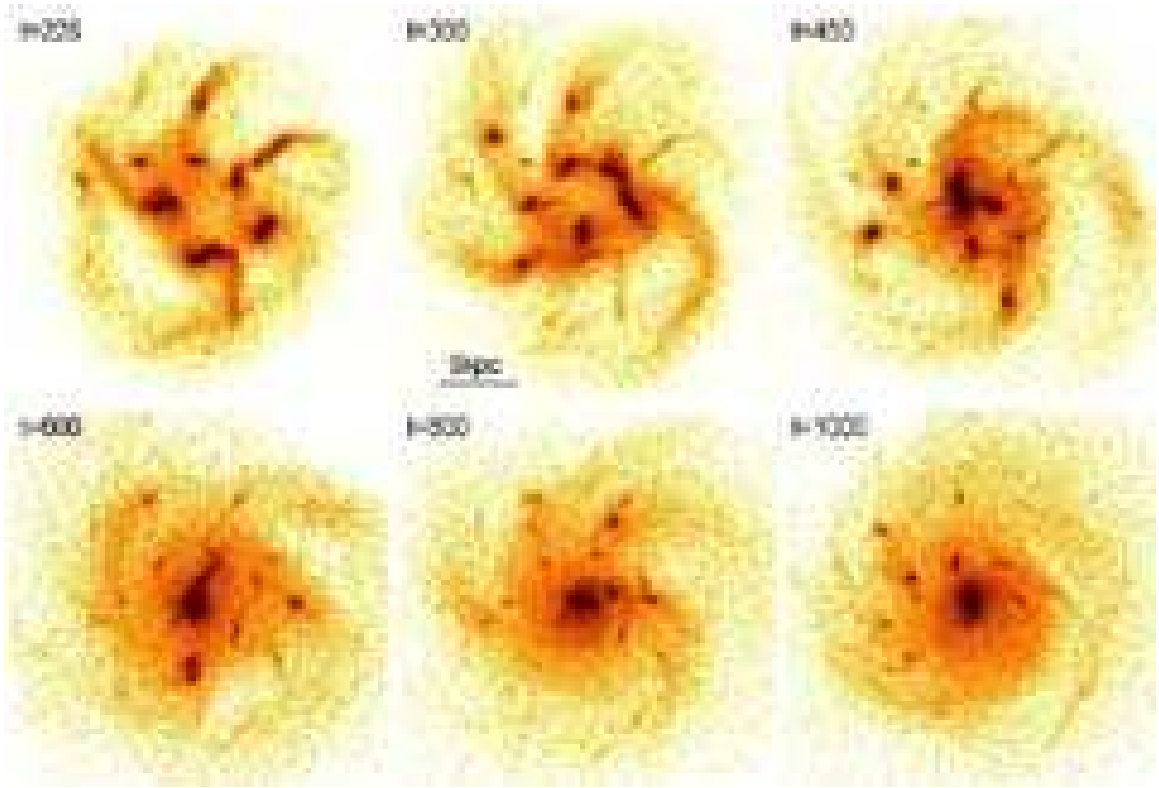

Fig. 3.— Same as Fig. 2 but for run 0B, where a primordial bulge of 10% of the disk mass is initially present in the model. The initial bulge stars are not shown here; only the gas and stars from the initial disk are shown. [Image degraded for astro-ph]

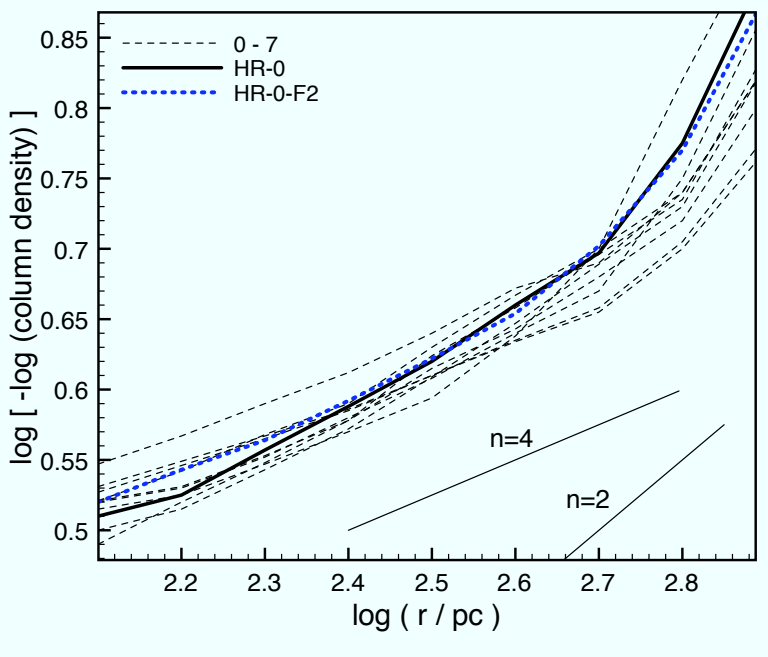

Fig. 4.— Normalized column density profile in the inner 800 pc plotted so that the slope is inversely proportional to the Sersic index, n. The bulge profiles have a high Sersic index at radii of 100-500 pc, indicating they resemble classical bulges. The thin dashed lines are runs 0 to 7, the thick solid line is run HR-0 (higher resolution) and the thick dotted line is run HR-0-F2 (supernova feedback).

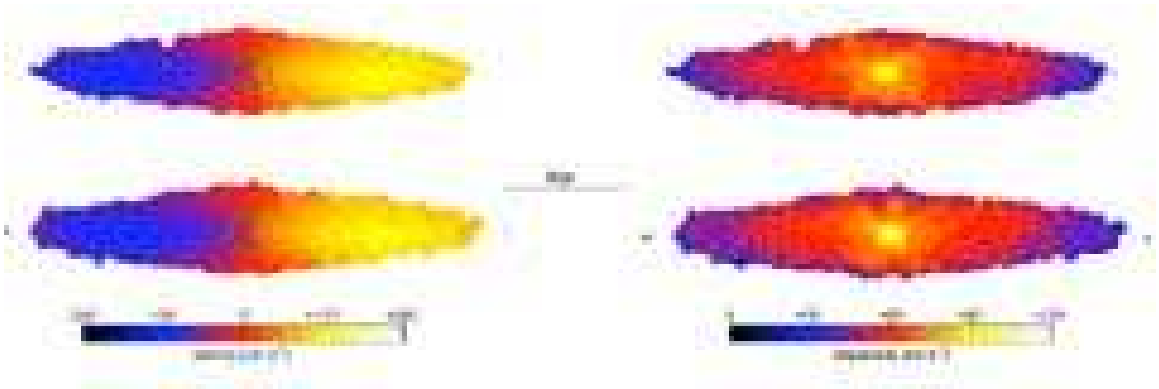

Fig. 5.— Line-of-sight velocity (left) and velocity dispersion(right) maps for two orthogonal projections of run 0 at the final stage. The green circles have a radius of 750 pc, which contains about two thirds of the bulge mass. The central regions have high velocity dispersions and slow rotations, indicating that clump coalescence is like a major merger with a randomization of orbits and a loss of angular momentum to the disk. [Image degraded for astro-ph]

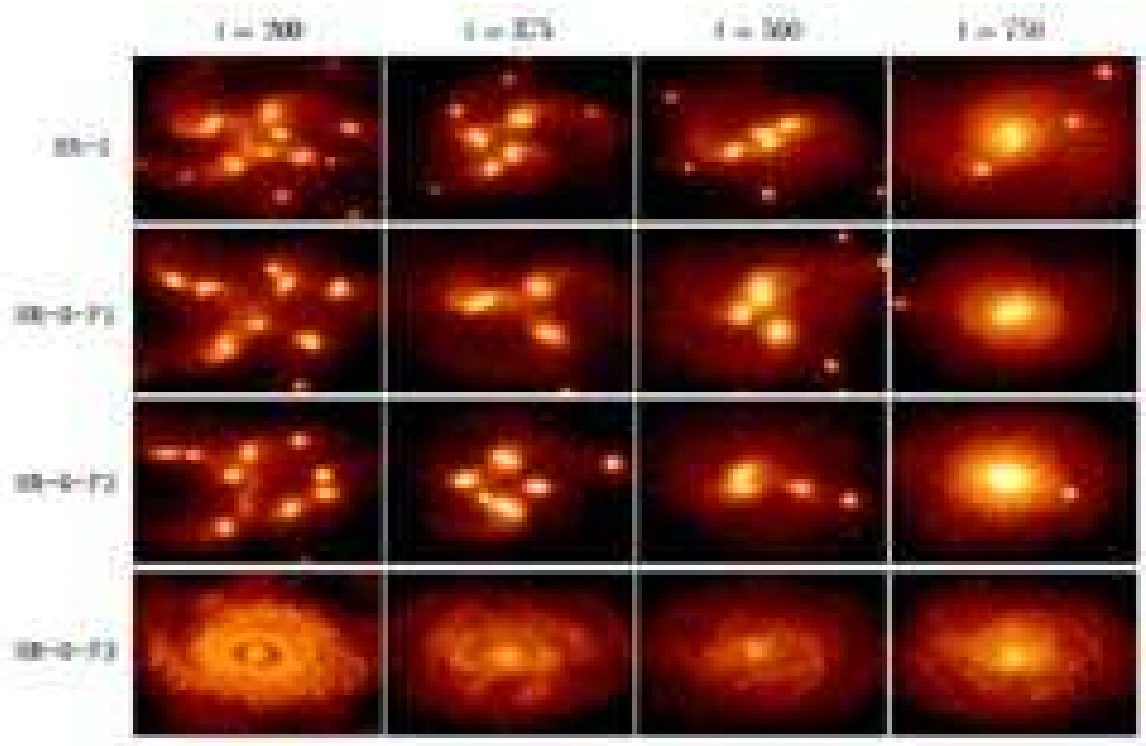

Fig. 6.— High-resolution models without (top) and with supernova feedback. The feedback efficiency increases from the second row to the bottom row, with such a high efficiency in the run HR-0-F3 that all star-forming clumps are rapidly destroyed. The snapshots show 30-degree projections of the total mass density, in log scale, and are 14×8 kpc wide. [Image degraded for astro-ph]

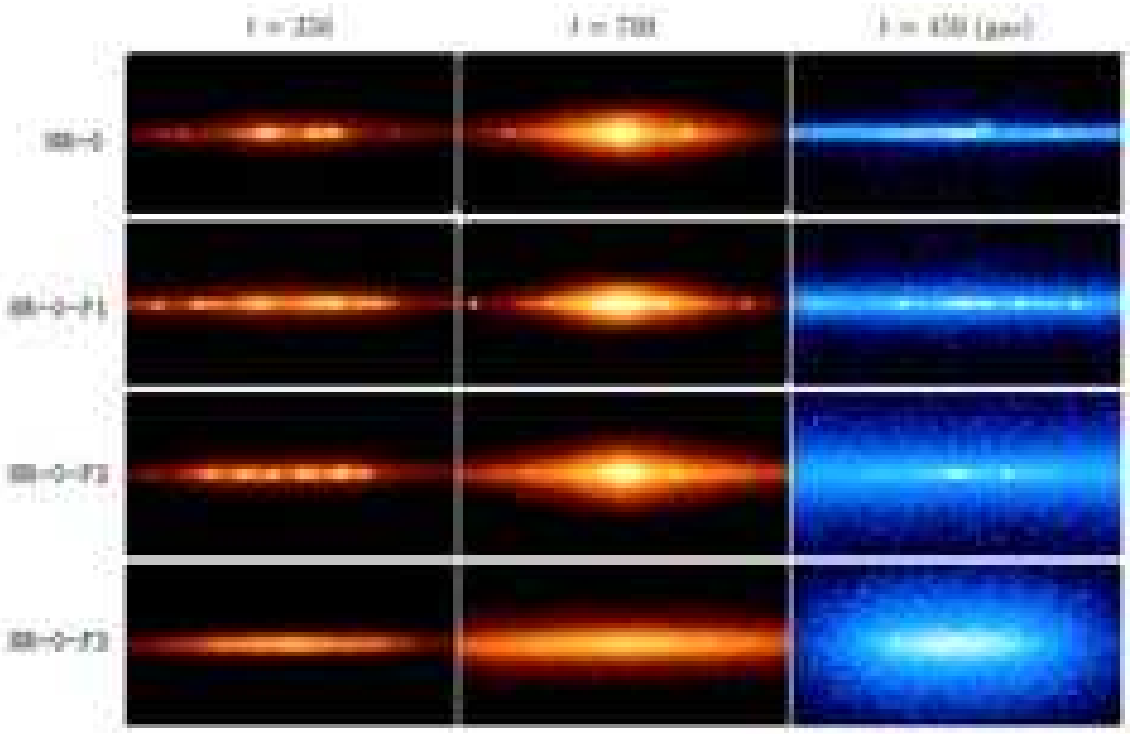

Fig. 7.— High-resolution models without (top) and with supernova feedback in edge-on projections, for the stellar mass density at $t = 350$ and 700 Myr, and for the gas mass density at $t = 450$ Myr. The snapshots are in log scale, and are 15×7 kpc wide. [Image degraded for astro-ph]

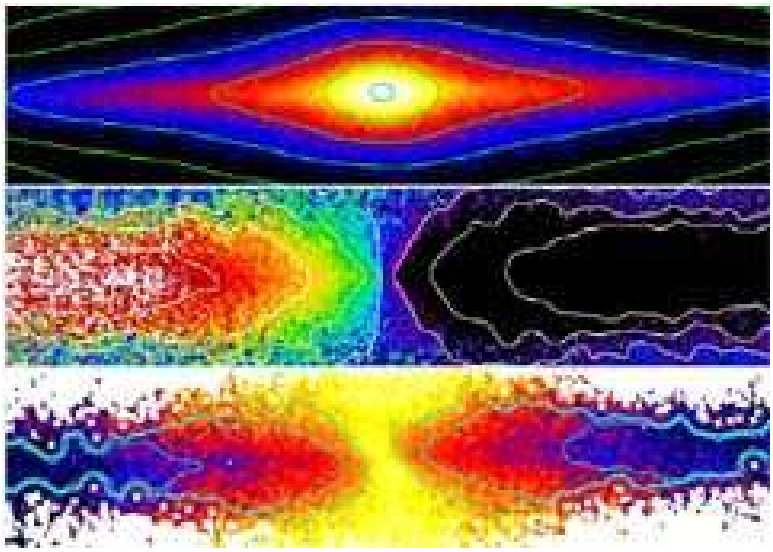

Fig. 8.— Edge-on view of the bulge in the high-resolution run HR-0 at the end of the simulation ($t = 1.3$ Gyr). The snapshots show the mass density (top), velocity field (middle) and line-of-sight velocity dispersion (bottom). Contours on the velocity field are at $V = 0$, ± 35, ± 70 and ± 105 km s^{-1}; $\sigma = 40$, 70, and 100 km s^{-1} on the dispersion map. Comparable results from a low resolution run were shown in Fig. 5. [Image degraded for astro-ph]

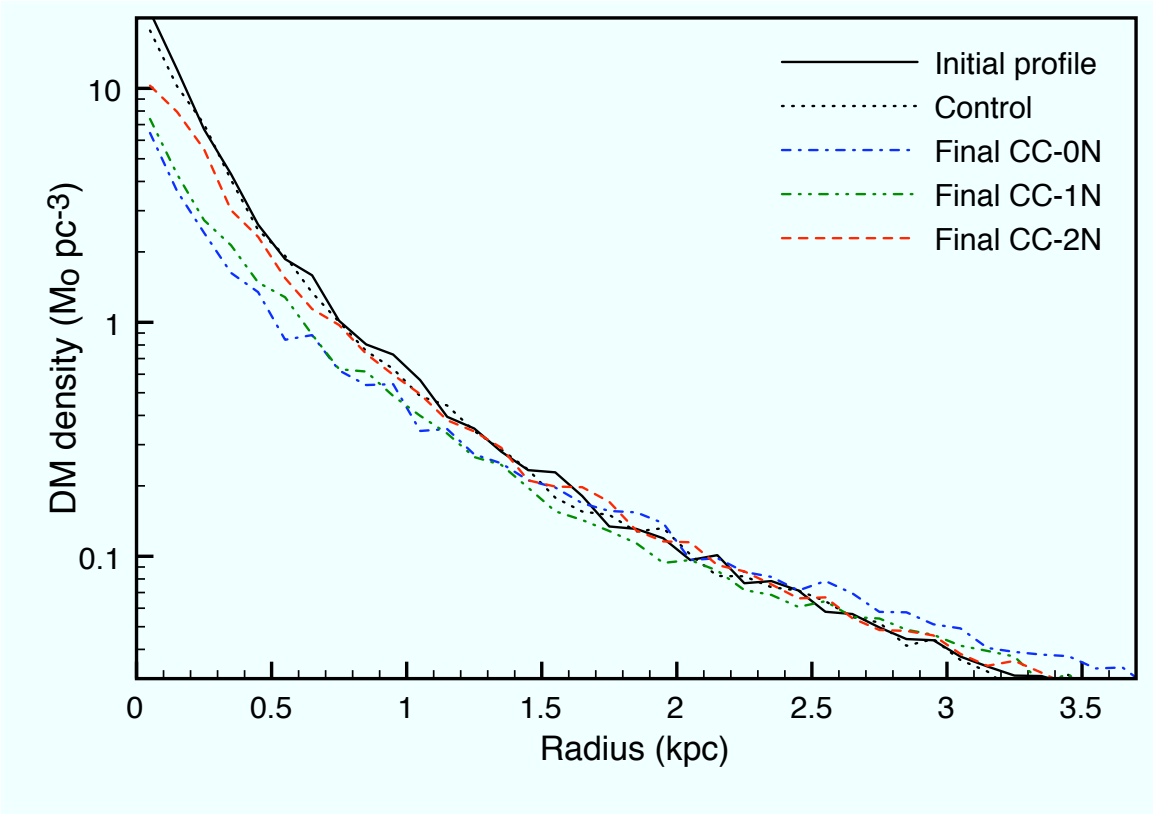

Fig. 9.— Density profiles of the dark matter in the three simulations started with NFW haloes (solid line). The three final profiles are at 1 Gyr, when the clumps have finished there migration, disruption and merging. The control run is with a rigid disk potential, showing that the profile evolution on the other runs is not a numerical artifact from the relaxation of the model halo, but caused by the clump-cluster evolution. The final profiles have a lower central peak density and somewhat larger scale-length, but are still cuspy.